A STABILITY ASSESSMENT OF COASTAL CLIFFS USING DIGITAL IMAGERY

Igor Ružić
University of Rijeka,
Faculty of Civil Engineering
Radmile Matejčić 3, HR-51000 Rijeka, Croatia
E-mail: igor.ruzic@uniri.hr

Čedomir Benac
University of Rijeka,
Faculty of Civil Engineering
Radmile Matejčić 3, HR-51000 Rijeka, Croatia

Ivan Marović
University of Rijeka,
Faculty of Civil Engineering
Radmile Matejčić 3, HR-51000 Rijeka, Croatia

Suzana Ilić
University of Lancaster,
Lancaster Environment Centre
LA1 4YQ Lancaster, United Kingdom

Abstract

The investigated area around the Stara Baška settlement (the island of Krk, NE channel part of the Adriatic Sea) is in a delicate geodynamic balance. Marine erosion is quite prominent and the recorded cliff retreat between 1966 and 2004 was from 4 to 5 metres. The cliff slopes are formed in talus breccias. Strong waves and formations of wave-cut notches are the main causes of the cliff's instability. The secondary causes are the weathering and erosion of the soil and rocks on the cliff. The slump of the cliff slope can occur in a rock mass with higher strength parameters, where the notches are cut a few metres inward into the toe of the cliff slope. A combined method for the stability analysis of the coastal cliffs was tested; this incorporates the cantilever-beam model and the structure-from-motion (SfM) photogrammetry. This method can provide highly detailed 3D geometrical data of the cliff, which can then be used in the calculations of the stability model. This is particularly important in a stability analysis of lithologically heterogeneous rocks such as breccias with varied geometry, which cannot be easily replaced by a rectangular surface. The simple and useful SfM method overcomes the limitations of traditional surveys in estimating the cliff overhang surface and the notch length.

1 INTRODUCTION

The occurrence and extent of coastal cliff erosion are primarily influenced by the lithology, the rock mass structure, and its geotechnical properties. These factors affect the local rates of retreat and the resulting cliff morphology (Grigss and Trenhaile, 1997). These have been the subjects of a number of studies. However, the erosion of hard rock cliffs has received less attention in previous studies due to their relative stability and generally slower rates of retreat than those found in soft rock cliffs. The recession of hard rock cliffs is usually the result of wave undercutting and the subsequent removal of debris deposited at the toe of the cliff by marine processes (Trenhaile, 2002). The most effective erosional processes take place near the water level, leading to the development of cliff notches at the base of the cliffs. These are then found to be responsible for cliff failure due to the imbalance of the forces and moments in the upper cliff-face material (Davies et al., 1991; Williams et al., 1993; Hungr et al., 2001; Matsukura, 2001; Castedo et al., 2012). Two main types of cliff mass movement are identified: topples and slides (Sunamura, 1992). Sub-aerial processes controlled by local climates such as seepage and surface run-off erosion can intensify the decay of the active coastal cliffs and hence their instability.

The cantilever-beam model has been used for a stability analysis of coastal cliffs with the presence of notches in a

number of studies (e.g., Thorne and Tovey, 1981; Abam, 1997, Matsukura, 1988, 2001; Kogure et al., 2006; Kogure and Matsukura, 2010; Castedo et al., 2012). The model is based on the assumption that the cliff-overhanging material above the notch acts as cantilever-beam load. The tensile stresses, which are distributed on the upper section, and the compressive stress, distributed on the lower section of the cliff face, are derived from the model (Timoshenko and Gere, 1972). To calculate the stresses, input parameters such as the rock density and the geometry of the cliff face are required. So far the model was mainly used to estimate the instabilities of the slopes in cliffs formed in jointed limestones (Kogure, 2006). In that case the cliff and the fallen block cross-sections have a roughly rectangular shape, which can be simply represented by a simple rectangular geometry (Kogure and Matsukura, 2010). The cliff's cross-section is calculated by multiplying the average cliff height by the horizontal distance between the retreat point of the notch and the averaged location of the cliff face.

In the case where the cliffs were formed in lithologically heterogeneous rocks, such as breccias, the cliff profiles have an irregular shape and no visible mechanical discontinuities and hence the geometry parameters, such as averaged cliff-face location, are difficult to define. Some authors (Williams et al., 1993; Kogure and Matsukura, 2010; Castedo et al., 2012) argue that a precise coastal 3D topography is needed for the cliff-stability analysis and the safety-factor determination. Field measurements of the 3D topography are extremely difficult to obtain and in some cases almost impossible due to the restricted access to the site and the risk of a cliff collapse. Moreover, the notch geometry is often difficult to measure with traditional instruments due to its substantial lengths and low heights. Also, a GPS-RTK device often does not work in such confined spaces. Remote sensing methods that overcome these problems have been mainly focused on analysing historical aerial photos and satellite images until recently. These, together with a traditional survey of the location of cliffs tops, have been used to estimate the amount and the cliff-retreat rate (Kuhn and Prüfer, 2014). However, these methods are not sufficient to derive the cliff geometry necessary for the stability models described above.

The new methods for topographic-data acquisition, such as LIDAR and those based on structure-for-motion (SfM) photogrammetry (James et al., 2013), enable the collection of high-accuracy and high-density 3D spatial data for researching the coastal geomorphology. The advantage of the SfM method in comparison with LIDAR, and other traditional photogrammetric methods, is that the images can be taken with a readily available, single digital camera such as 10-megapixel

Ricoh GR Digital IV. Multiple photographs are taken from various horizontal and vertical angles (James and Robson, 2012). Unlike traditional photogrammetric methods, which need the 3D location and position of the camera(s), the SfM method solves the problems of camera position and scene geometry simultaneously and automatically by using a highly redundant bundle adjustment based on matching features in multiple overlapping, offset images (Snavely et al., 2008; Westoby et al., 2012). It has been demonstrated that this simple method is highly applicable for studies of gravel beach dynamics (James et al., 2013) at the Uboka pocket beach (Fig. 1, location 2), changes in beach slopes at the gravel beach and erosional processes in talus breccia (Ružić et al., 2013) in Mošćenička Draga (Fig. 1, location 3) and cliff geomorphology (Ružić et al., 2014) at the site of Stara Baška (Fig. 1, location 1).
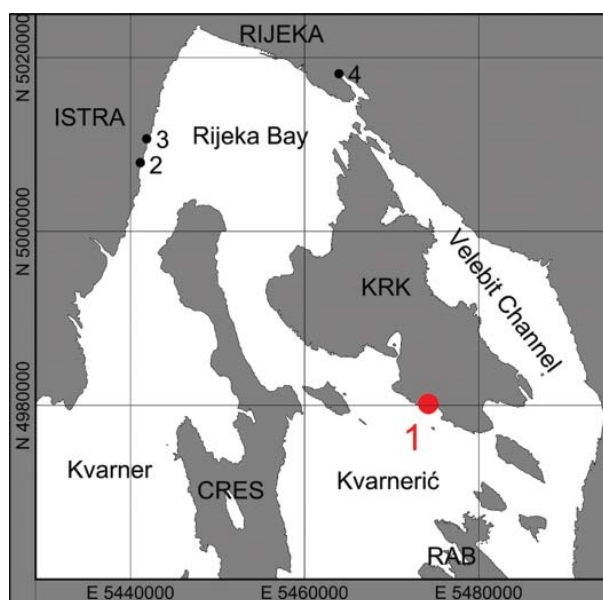

Figure 1. Study area with the location of Stara Baška (1); locations of previous researches in Uboka (2), and Mošćenička Draga (3) and the location of mareograph (tidal gauge) Bakar (4).

The north-eastern Adriatic coast is predominantly a steep, rocky coast formed of karstified carbonate rocks, compared to the flat south-western Italian side. For this reason, the geomorphology of this coastal area is more complex and diverse, comprising a number of coastal forms on a small scale (Pikelj and Juračić, 2013).

The coastal cliffs near Stara Baška in the Kvarner Bay area in Croatia (Fig. 1, location 1, Fig. 2) are made of talus breccias and have pronounced notches. These cliffs are very unstable and have significantly retreated during the past five decades and collapsed rocky blocks are often found on the beaches fronting the cliffs. Some of the island`s impor-

tant infrastructure, such as the tourist camp in Stara Baška, is threatened by these cliff collapses. Hence, a prediction of this type of geohazard is extremely valuable for future spatial planning and development on this coastline.

The aim of this paper is to examine the stability of the breccias cliffs at the site in Stara Baška using the cantilever-beam model (Kogure et al., 2006) in combination with the SfM method, which is used to derive the geometrical properties of the cliffs. We examine the effect of notches on the distribution of the stresses inside the cliffs as well as on the spatial distribution of the stresses along the cliff face. The advantage and limitations of both methods are illustrated as well as the recommendation for further studies.

2   BACKGROUND TO THE INVESTIGATED SITE

The area around the Stara Baška settlement has a delicate geodynamic balance, and the coastal cliff's erosion is intense. The coastal geomorphology, shown in Figure 2, consists of several headlands and embayments. The figure also shows the settlement of the village itself and the camping site on the top of the cliffs.

2.1   Geomorphology and geological setting

The Kvarner area, a semi-enclosed section of the Adriatic Sea, is located between the Istrian peninsula and the Vinodol-Velebit coast. Geographically, the island chains Cres-Lošinj and Krk-Rab-Pag divide it into the Rijeka Bay; the Kvarner Bay, Kvarnerić; and the Velebit Channel (Fig. 1). Intensive morphogenetic processes caused by tectonic movements and rapid sea-level changes, as well

as climatic changes, resulted in the present shape of the Kvarner area, as well as the shape of Krk Island (Benac and Juračić, 1998; Benac et al., 2013).

In the terrestrial part of the Kvarner area, sedimentary carbonate rocks prevail, whereas siliciclastic rocks are rare. Pleistocene and Holocene deposits locally cover this bedrock substrate. The waves in the channel part of the northern Adriatic Sea are not as high as in the western open zone due to the relatively short wind fetch. On a carbonate rocky coast bio-erosional processes prevail over mechanical erosion and tidal notches are common features of these processes. In places where the rock mass is tectonically crushed or karstified, wave-notches and cliffs evolved. Marine erosion and more rapid cliff recession are obvious in a less-resistant siliciclastic rocky coast and Pliocene-Quaternary sediments (Juračić et al., 2009).

The area surrounding Stara Baška consists of Upper Cretaceous and Palaeogene carbonate rocks. Palaeogene siliciclastic rocks such as marls and flysch outcrop can be found in a relatively narrow coastal zone. They are mostly covered by Pliocene-Quaternary sediments (Benac et al., 2013). The carbonate rocks, such as limestone, dolomitic limestone and dolomitic breccia, have a different degree of fissuring and form a typical bare karstic landscape. Research was focused on two embayments carved into Pliocene-Quaternary talus breccias (Fig. 2). The outcrops of flysch rocks are partially visible in the narrow coastal zone.

Site research showed that breccias have pronounced horizontal stratification and the joints were not visible. Horizontal layers consist of limestone fragments/clasts from a few millimetres in size to blocks greater than 50
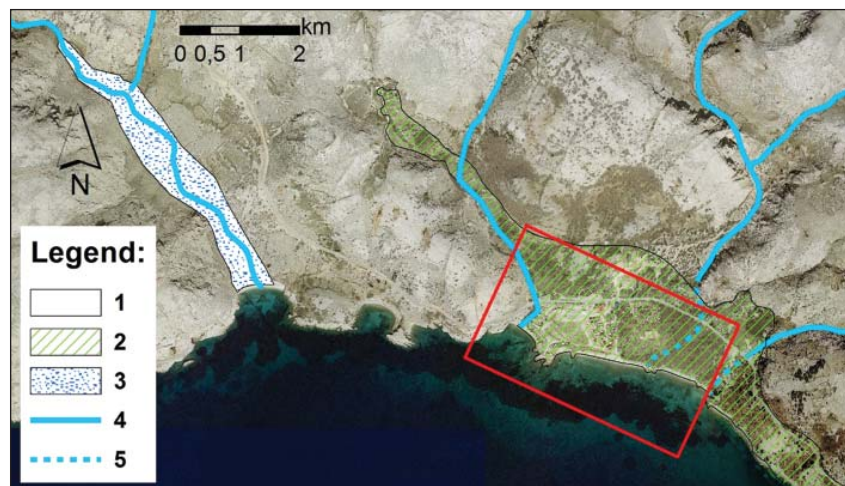

Figure 2. Simplified engineering geological map of the investigated area (red rectangle): 1-carbonate rocks (Upper Cretaceous and Palaeogene limestones), 2-siliciclastic rock mass (Palaeogene marls and flysch) mostly covered by Quaternary talus breccias, 3-Quaternary alluvial sediments, 4-periodical surface water flow, 5-partially canalized water flow.

cm, with prevailing fragments of 1–4 cm in size. The matrix is reddish silt-sandy cement (20–50% clay) with a different degree of calcification. A different degree of calcification has a great influence on the erodibility as well as on the strength parameters of breccias.

Cliffs formed in talus breccias have an average height of 5 to 6 metres. The top layer at the subsurface, of about 1 m thickness, is completely weathered and has soil features. These features are clearly visible in the block fallen from the cliff, as shown in the photo taken during one of the field visits (Fig. 3). On the beach in front of the cliffs, gravel and partially coarse sand sediments prevail. The average gravel grain size is between 2 and 20 mm.

Figure 3. Recently collapsed cliff (09/01/2014), site location 1 (SL1): 1 - soil (like weathered zone), 2 - talus breccia.

2.2 Climatic conditions

Low and moderate winds intersected with silent periods are most frequent, while storm winds (speed > 30 m/s) are rare (Leder et al., 1998). North-eastern wind bora is predominant and reaches a maximum speed of 30 m/s. The mean sea level recorded at the nearest tidal gauge in Bakar (Fig. 1, location 4) is 0.15 m (vertical datum of the Republic of Croatia - CVD). This is a micro-tidal environment with a tidal range between 30 and 35 cm (Benac et al., 2004). The Kvarner area is a semi-enclosed section of the Adriatic Sea between the Istrian peninsula and the Vinodol-Velebit coast. This affects the increase in water levels and wave heights during storms. The storm surge can increase the water level up to 1.18 m CVD, as recorded in Bakar on 1 December 2008. The 100-year return and the 1-year return periods of the storm surge levels are 1.30 m CVD and 0.80 m CVD, respectively (Ružić, 2003). The wave heights in the Kvarnerić area near Stara Baška are smaller than in the western open zone due to the relatively short wind fetch. Hence, the

north-eastern bora forms moderate waves due to small fetches, despite having the highest speed. South-east winds generate the highest waves, as shown in Figure 4.

Figure 4 shows significant wave-height simulations using the SWAN model (Booij et al., 1999). The wave simulation was performed for a SE wind speed of 25 m/s (100-year return period). For illustration purposes, the model assumes a uniform distribution of wind over the domain and does not take into account the complex wind field in the Bay. The area around the Stara Baška settlement has an approximately 25% lower significant wave height than the exposed opposite channel part (Fig. 4).
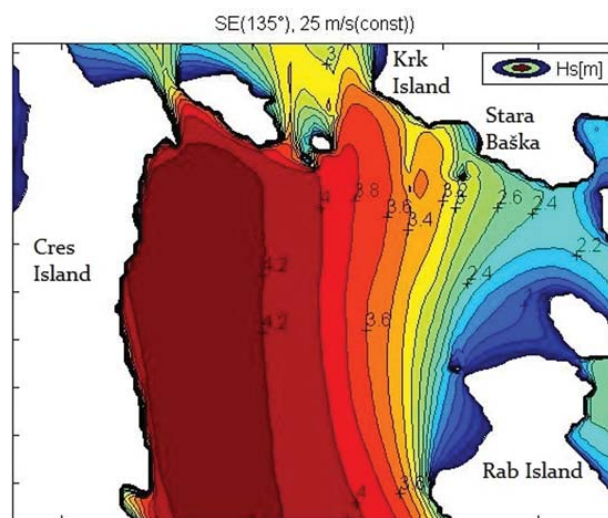

Figure 4. Significant wave height (in metres), NE part of Kvarnerić (according to the SWAN wave model).

2.3 Evidence of cliff retreat

The analysis of historical aerial images showed that the breccias are prone to rapid cliff recession (Ružić et al., 2014). The changes in the cliff-top position were identified by a comparison of geo-referenced aerial images from 1966 and ortho-rectified photos from 2004, shown in Figure 5. Autodesk RasterDesign software was used for the georeferencing. The georeferenced map's estimated horizontal accuracy is up to 0.50 metres due to the distortion of the old areal images. Visible changes were noticed between these two aerial surveys. Furthermore, large rocky blocks situated at the toe of the cliffs indicate earlier local block falls.

In the western embayment, a significant cliff retreat of up to 5.5 m is found only in the eastern part (Fig. 5c, near profile 2). This resulted in an increase of the beach area by about 75 m^2. The cliff line in the middle part of the embayment (Fig. 5c, profile 1) did not change significantly. In this case, the detected changes are smaller than the possible errors in the image analysis. In the
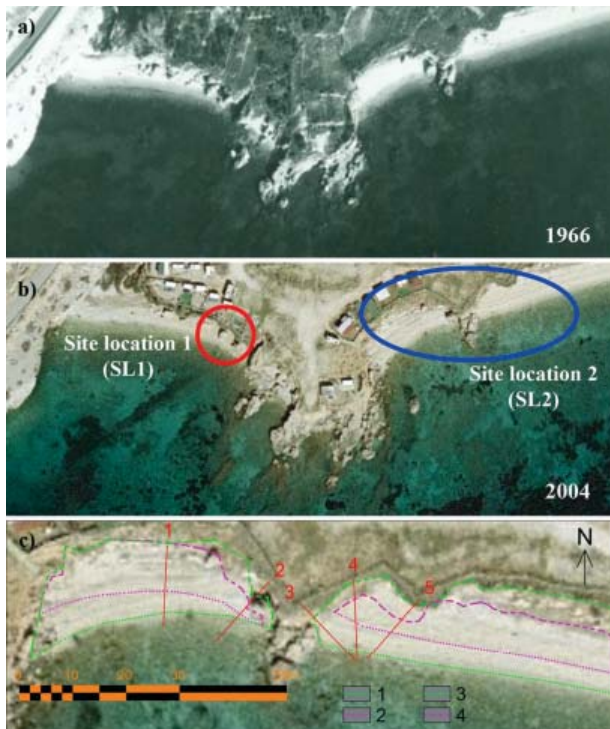
Figure 5. Aerial photographs showing considerable coastal changes between 1966 and 2004: a) geo-referenced aerial photo from 1966; b) ortho-photo map from 2004; c) coastal changes between 1966 and 2004: 1 - coastline 2004; 2 - coastline 1966; 3 - cliff line 2004; 4 - cliff line 1966. Red line and numbers (Fig. 5c) indicate analysed profiles.

eastern embayment, the retreat in the cliff-top location is up to 5 meters at the western side (Fig. 5c, profiles 4 and 5). The cliff near profile 4 has retreated by about 2 metres since 1966. The beach area increased here up to 265 m^2. This analysis showed that the cliff's retreat results in an extension of the beach area. Also, it showed that there is a noticeable spatial difference in the cliff retreat, which will be explained later. The stability of the cliffs at the locations identified here will be further investigated by using the combined cantilever-beam model and the SfM method.

3 METHODS

For the stability analysis, the cantilever-beam model given by Kogure et al. (2006) is adopted and briefly summarized here. Kogure et al. (2006) assessed a cliff-failure process based on three stages: (1) a developing of notch forms as a column like a cantilever beam; (2) this column generates tension cracks on the top surface of the cliff due to the tensile stress arising from its own weight; and (3) a vertical extension of the cracks causes bending failure of this column-shaped mass, which results in a toppling mode of failure.

Point-load tests were carried out using a *Digital rock strength index apparatus* (Control 45-DO550/D). The density in dry and wet conditions of the selected samples in talus breccia has been measured according to standard methods (HRN EN 1097-6). The estimation of the Geological Strength Index (GSI) has provided us with the according standard methods (Hoek and Brown, 1991; Hoek, 1996; Marinos and Hoek, 2000).

The maximum bending stress (σ_{max}) inside a cliff is estimated as the ratio of the bending moment (M) and the modulus of the cliff section (Z) given in Equation 1.

$$\sigma_{max} = \frac{M}{Z} \qquad (1)$$

$$M = \frac{1}{2}\rho g b h_c l_n^2 \qquad (2)$$

$$Z = \frac{1}{6}b h_c^2 \qquad (3)$$

Equations 2 and 3 are used to estimate the bending moment and the modules for a cliff section with breadth (b), height (h_c) and notch depth (l_n), respectively. The cliff height (h_c) is defined as the vertical distance between the retreat point of a notch (the deepest point of a notch) and the top surface of a cliff. The notch depth l_n is defined as the horizontal distance between the retreat point of a notch and an averaged cliff face. For cliffs with tension cracks present on the top of the cliff, only the height that experiences the tensile and comparative stresses would be taken into account. Figure 8 shows the stress distribution inside a cliff with no tension cracks (Fig. 8a) and with tension cracks (Fig. 8b).

A structure-from-motion (SfM) photogrammetric method was used to obtain parameters such as the area of the cliff-overhang material, the height of the cliff face and the length of the notch (Ružić et al., 2014). These are derived from geo-referenced 3D point clouds generated from approximately 200 images using the Autodesk ReCap online service (https://recap360.autodesk.com/). The images were collected using a single 10-megapixel Ricoh GR Digital IV camera equipped with a high-contrast 6-mm f/1.9 GR lens, and focusing on embayments as shown in Figure 5b (i.e., SL1 and SL2). Special care was needed to acquire sharp and well-focused images from a variety of locations covering a range of vertical and horizontal angles. Also, visual checks were used to select images to upload to the Autodesk ReCap online service and for 3D point cloud verification, as suggested by Podobnikar (2009). Cloud Compare software (http://www.danielgm.net/cc/) was used for the point cloud geo-referencing. A small number of ground-control points (GCPs) were measured in the field using Real Time Kinematic GPS (RTK-GPS) after the images were taken. These

were then used for the transformation of coordinates from a relative to an absolute coordinate system (e.g., Westoby et al., 2012). It is important to point out that all the images were taken within a period of less than two hours. Complete field measurements, including RTK-GPS surveys, took about six hours for a two-person team.

4 RESULTS

4.1 Properties of the material in the cliff

The stability analysis was based on laboratory-derived data. The material bulk density in dry conditions is 24.5 kN/m^3, and 25.3 kN/m^3 in wet conditions. The uniaxial comprehensive strengths are USC = 29.21–70.21 MPa in dry conditions and USC = 19.82–62.10 MPa in wet conditions. The estimated Geological Strength Index is GSI = 25–35, and the internal friction angle is F = 28–35° (mi = 20) (Hoek and Brown, 1991; Hoek, 1996; Marinos and Hoek, 2000).

It is difficult to estimate the geological parameters in lithologically very heterogeneous rocks like breccia. A correlation between the heterogeneous breccias compressive and tensile strengths cannot be unambiguously defined.

4.2 Cliff geometry derived from the photogrammetry

An example of a high-density 3D point cloud, derived from a set of photo images taken on the sites SL1 and SL2 are shown in Figure 5. Different parts of a cliff and beach, such as the cliff face, notches, vegetation on the top of the cliff, the upper and lower beach, and their structures are clearly identifiable from the cloud. The locations of the cliff and notches and their geometrical properties are obtained from a geo-referenced 3D point cloud. The spatial variation in the cliff geometry is clearly illustrated in Figure 6. The high-resolution of the images and the colour provide additional information about the spatial variation of the cliff geomorphology and the vegetation cover.

Cliff cross-sections obtained from a geo-referenced point cloud at a number of locations marked in Figure 6 are

shown in Figure 7. All the profiles have vertical convex cliff faces fronted by a gently sloping beach. They can be categorized as those that do not have notches (Profiles 1 and 4) and those with pronounced notches and a cliff overhang (Profiles, 2, 3 and 5). For Profile 1 the cliff base is at 1.8 m above sea level and a half metre above the 100-year storm surge level. The beach width taken from the mean sea level to the toe of the cliff is 11.4 m. For Profile 4 the cliff base is 1.2 m above the sea and the beach width is 5.5 m. The cliff notch is not visible from the derived cliff profile. However, the photorealistic 3D point cloud (Fig. 6) indicates that the cliff undercut is filled with sediments.

The cliff profiles 2, 3 and 5 have pronounced notches at the cliff toe. The 100-year surge water level reaches the notches at Profiles 2 and 3, but this is not the case with Profile 5, which is about 40 cm above it. The beach width is 5.6 m and 0.8 m in Profile 2 and Profile 3, respectively. The largest width of the beach is 7.7 m, found at Profile 5.

4.3 Results of stability analysis

The cross-section geometry derived from the SfM photogrammetry was used to calculate parameters such as the cliff area, the cliff overhanging material weight and the centre of gravity. These are then used in the cantilever-beam model for an estimation of the cliff's maximum bending stress (σ_{T-max}) using equation 1. The wet density of breccias of 25.3 kN/m^3 was taken into account. The estimates for profiles 2, 3 and 5 are given in Table 1 (row 11) and Figure 8a illustrates the distribution of stresses for Profile 3.

The stresses are calculated by considering the 'proper' area of the profile rather than a rectangular approximation in the momentum equation (2). These are given in Table 1 in the 15th row. All the profiles' calculations of stresses are corrected for the presence of a soil layer on the top of the cliff. As the soil does not support tensile stresses, it leads to an increase of the tensile and compressive stresses in the underlying rock. These increased stresses were calculated following Kogure et al.'s (2010) approach for cliffs with pronounced cracks. The method reduces the critical height of a cross-section
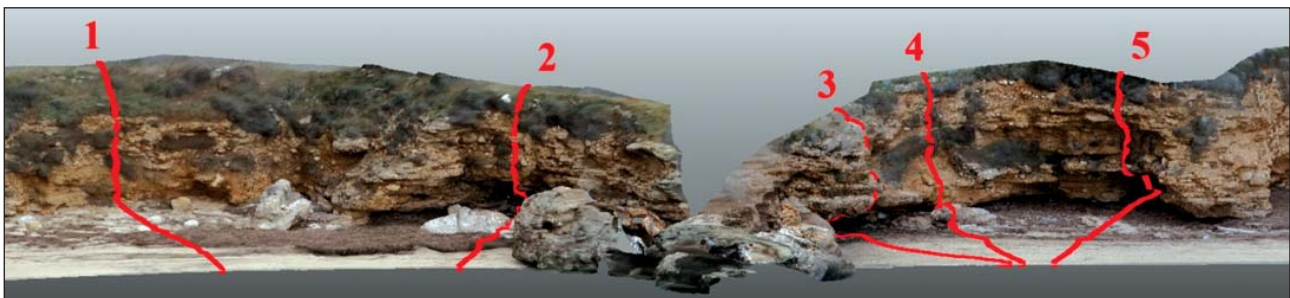

Figure 6. Photorealistic 3D point clouds shown from different angles with marked profiles (red lines)-
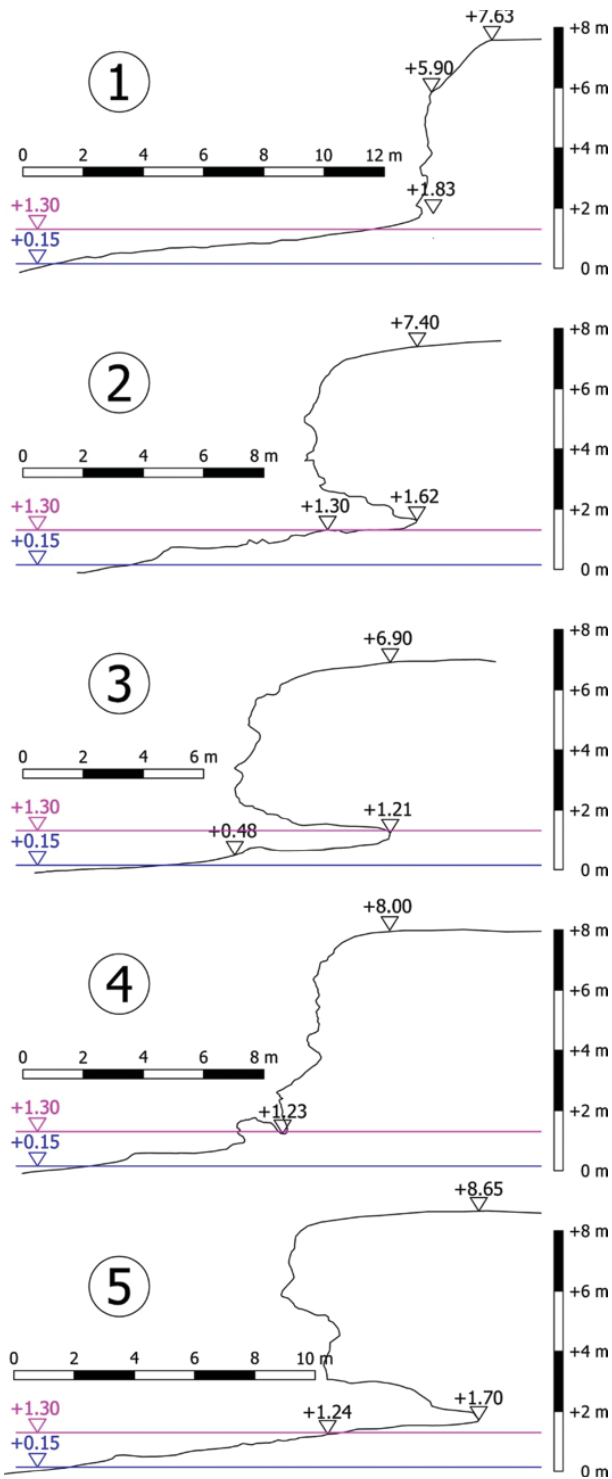
Figure 7. Cross-sections perpendicular to the coastline, profiles 1–5 (Figs.6 and 10); characteristic sea levels: mean sea level (blue) and 100-year storm surge (magenta).

Figure 8. Stress distribution inside a cliff (profile 3) with no tension crack (a) and with a tension crack – soil layer (b), and the main variables used in the calculation.

the depth of the top soil layer was estimated to be 1 m (as shown in Fig. 8), and the critical height was reduced accordingly (Table 1, row 13).

4.4 Distribution of stresses along the cliff face

The detailed cliff geometry derived from the point cloud allowed precise geometrical parameters for the spatial distribution of the stresses along the cliff face. The section around Profile 3 was considered, as it has the widest cliff notch and may be considered as a 3D phenomenon.

Two cross-sections on each side from the current Profile 3, with a 2 m offset between them, were chosen (Fig. 9a) for a stability analysis. Figure 9b shows the difference in chosen profiles in terms of the notch length and the cross-sectional area.

Table 2 gives a summary of the estimates, parameters and calculated values for all the cross-sections. The largest stresses are found between profiles 3–3 (0.352 MPa/m[1]) and 3–4 (0.356 MPa/m[1]). The section stresses decrease approximately 16 times between profiles 3–4 and 3–5, the distance of which is only 2 metres. This clearly correlates with the length of the cliff notches, which is the deepest between profiles 3–2 and 3–4.

for a tensile crack depth. Here, the critical height of a cross-section was reduced by the thickness of a soil layer (Fig. 8b). From the 3D point cloud shown in Figure 6,
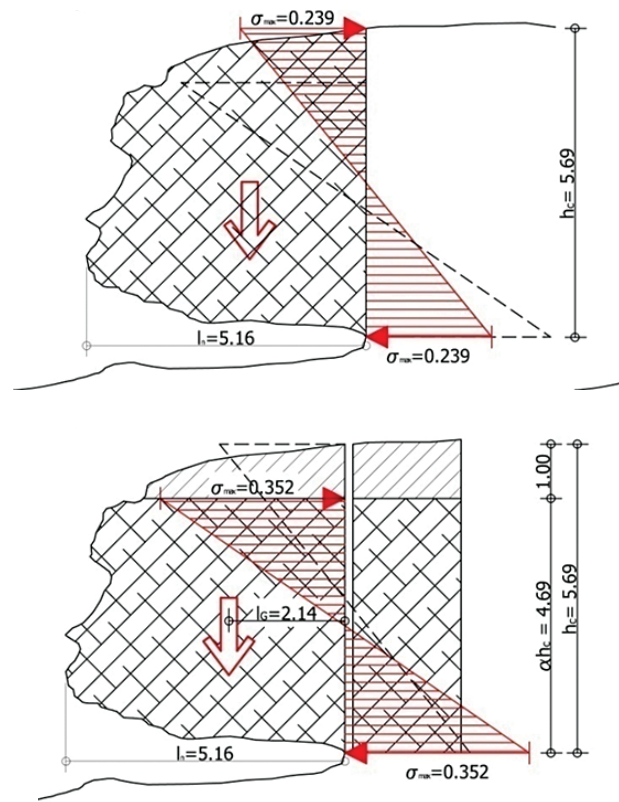
Table 1. The cliff (beam) model input parameters and the resulting sections stress.

	Property	Symbol	Unit	Profile		
				2	3	5
General properties	Bulk density	γ	kN/m³	25.30	25.30	25.30
	Cliff area	A	m²	16.20	23.04	33.09
	Notch depth	l_n	m	3.73	5.16	6.56
	Centroid distance	l_G	m	1.56	2.21	2.71
	Cliff weight	G	kN/m¹	409.90	582.90	837.10
	Momentum	M	kNm/m¹	640.70	1290.60	2269.20
	Cliff height	h_c	m	5.78	5.69	6.92
Without crack (soil not taken into account)	Depth of tensile crack	αh_c	m	0.00	0.00	0.00
	Bearing cross-section height	$h_c - \alpha h_c$	m	5.78	5.69	6.92
	Centre of masses	Z	m³	5.57	5.39	7.98
	Tensile stress	σ	kN/m²/m¹	115.10	239.30	284.30
With crack (soil taken into account)	Depth of tensile crack	αh_c	m	1.00	1.00	1.00
	Bearing cross-section height	$h_c - \alpha h_c$	m	4.78	4.69	5.92
	Centre of masses	Z	m³	3.81	3.66	5.84
	Tensile stress	σ	kN/m²/m¹	168.20	352.40	388.50

Profiles 3–1 and 3–5 are the cliff-boundary profiles, the cliff overhanging material area and the section height ratio is restricted and its stresses are limited (0.035 and 0.023 MPa/m¹). The tensile stresses are in places larger than 300 kN/m³, which are approaching the critical stresses for these types of rocks. It is also shown that this combined method can identify much closer locations with maximum stresses. The strength of the tensile stresses and their distribution result in a non-uniform cliff recession, also seen from the analysis of the historical aerial photographs.

5 DISCUSSION

Assuming that the cliff collapse is solely the result of the notch length and amount of material overhanging the

notch, the proposed combined method could be useful for estimating the stresses in the cliff face and its stability. In particular, it is shown that the use of the SfM method can examine a number of cliff profiles at different spatial distances in order to identify a critical profile. So far, the stability analysis was based on a limited number of cliff profiles and was very much dependent on the subjective choice of a critical profile when taking measurements in the field. Another advantage is that we can estimate the length of the notch much more easily. As an illustration, the tensile stresses at Profile 5 are calculated by taking into account the 'assumed rectangular cliff area' and three different values for the notch length: the minimum, maximum and mean value, as suggested by Kogureet et al. (2006). Those stresses calculations are made by using the cliff height hc and the notch length ln following Kogure et al. (2006) and
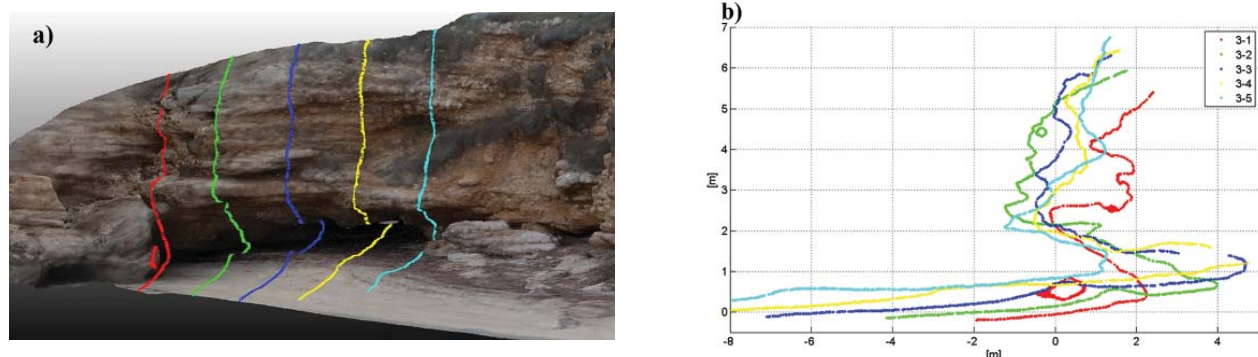

Figure 9. Cliff profiles (3–1 to 3–5 with an offset of 2m between each other) parallel to profile 3:
a) 3D point cloud; b) 2D profiles delivered from 3D point cloud.

Table 2. Tensile-stress calculation parameters from profile 3–1 to 3–5.

	Property	Symbol	Unit	Profile 3				
				3-1	3-2	3-3	3-4	3-5
General properties	Bulk density	γ	kN/m^3	25.30	25.30	25.30	25.30	25.30
	Cliff area	A	m^2	4.40	20.62	23.04	23.15	3.87
	Notch depth	l_n	m	2.35	5.21	5.16	5.42	2.46
	Centroid distance	l_G	m	0.73	1.97	2.21	2.20	0.68
	Cliff weight	G	kN/m^1	111.30	521.70	582.90	585.70	97.90
	Momentum	M	kNm/m^1	81.00	1027.70	1290.60	1286.70	66.80
	Cliff height	h_c	m	4.75	6.29	5.69	5.66	5.22
Without crack (soil not taken into account)	Depth of tensile crack	αh_c	m	0.00	0.00	0.00	0.00	0.00
	Bearing cross-section height	h_c-αh_c	m	4.75	6.29	5.69	5.66	5.22
	Centre of masses	Z	m^3	3.75	6.60	5.39	5.33	4.54
	Tensile stress	σ	kN/m^2/m^1	21.6	155.8	239.3	241.3	14.7
With crack (soil taken into account)	Depth of tensile crack	αh_c	m	1.00	1.00	1.00	1.00	1.00
	Bearing cross-section height	h_c-αh_c	m	3.75	5.29	4.69	4.66	4.22
	Centre of masses	Z	m^3	2.34	4.67	3.66	3.61	2.97
	Tensile stress	σ	kN/m^2/m^1	34.7	220.2	352.4	356.1	22.5

described in the previous section. The results are given in Table 3 (row 6) and there is a significant difference between these estimates. These are then compared with the calculated tensile stresses, taking the measured area into account. The difference is 29% when the mean notch length is taken into account. If the mean notch length ln is overestimated, differences might be even higher, as shown in Table 3. This again highlights the importance of obtaining accurate cliff-geometry parameters.

The SfM method can be used to estimate the depth of the top-soil layer on the basis of the colour difference in the 3D point cloud. However, these estimates are more uncertain as they are based on the information from the cliff front, which might have different settings than the cliff critical profile. It is not possible to obtain the depth across the profile from the images or, for example,

estimate the length of the cracks on the back of the cliff overhang. Figure 10 shows the maximum tensile stresses as function of a range of soil depths (0-2m). The estimates are calculated for Profiles 3–1 to 3–5. The cliff section tensile stresses increase significantly due to the increase of the soil cover thickness on the top of the cliff (Fig. 10, profiles 3-3 and 3-4). For example, an increase of 160% in the tensile stresses is obtained if the soil depth increases from 0 (no soil) to 1m. Hence, further work should focus on improvements to these estimates.

There are some limitations to this methodology, which will require further consideration in the future. An assumption was made that the density is constant along the whole cliff face, despite breccias being lithologically heterogeneous rocks and therefore having a spatially varied density. The density can also vary with time.

Table 3. The effect of the notch length on estimates of the tensile stresses.

			Profile 5		
Property	Symbol	Unit	ln_min	ln_max	ln_mean
Notch depth	l_n	m	5.02	6.56	5.79
Cliff height	h_c	m	6.92	6.92	6.92
Bulk density	γ	kN/m^3	25.30	25.30	25.30
Momentum	M	kNm/m^1	2206	3767	2935
Centre of cliff masse	Z	m^3	7.98	7.98	7.98
Tensile stress (equations 1-3)	σ	kN/m^2/m^1	276.40	472.00	367.70
Tensile stress (real area)	σ	kN/m^2/m^1	284.30	284.30	284.30
Tensile stress difference		%	-3%	66%	29%

So far the stability method, adopted here, does not take into account other parameters and effects that might influence the stability of cliffs. Secondary processes such as rock weathering, soil erosion and subaerial processes are not included. Furthermore, the method does not take into account processes that might influence the formation and stability of notches, such as wave impact, salt-water weathering, wetting and drying and beach sediment abrasion. Figure 7 illustrates that the sea level reaches the notches at several locations. The narrow gravel beach absorbs most of the wave's mechanical energy during normal conditions. However, during an extremely high water level, waves reach the cliff's toe and can contribute to the cliff's undercut formation and the cliff's retreat. According to the expected sea-level rise and more frequent events of extreme high water levels (Aqua Alta) in the Kvarner area (Antonioli et al., 2007), the sea level and waves will reach the cliff toe more frequently. This could contribute to the acceleration of marine erosion and cliff retreat. It is important to investigate how to incorporate the dynamic processes of changes in cliff geometry into the stability model.

6 CONCLUSIONS

The investigated area around the Stara Baška settlement is in a delicate geodynamic balance. The comparison of ortho-rectified aerial photos from 1966 and 2004 showed that marine erosion is quite prominent and the cliff retreat has been between 4 and 5 metres with a simultaneous expansion of the beach surface. The main cause of the cliff slopes' instability is the occurrence of strong waves and the formation of wave-cut notches. Secondary causes are the weathering and erosion of the soil and rocks on the slope surface of the cliff. The slump of the cliff's slope can occur in a rock mass with better strength parameters, where the notches are cut a few metres inward into the toe of the cliff slope.

The new combined method for the stability analysis of coastal cliffs was tested and had incorporated the cantilever-beam model and the structure-from-motion (SfM) photogrammetry. The SfM photogrammetry can provide highly detailed 3D cliff geometrical data, which can then be utilized with the stability model. This is particularly important in a stability analysis of rocks such as breccias with a varied geometry, which cannot be easily replaced by a rectangular surface. The SfM method overcomes the limitations of traditional surveys in estimating the cliff overhang surface and the notch length. It has been demonstrated that the tensile stresses estimated by using 'real' and 'assumed rectangular' cliff areas may differ significantly.

Acknowledgements

REFERENCES

[1] Abam, T.K.S. 1997. Genesis of channel bank overhangs in the Niger Delta and analysis of mechanisms of failure. Geomorphology 18, 2, 151-164.

[2] Antonioli, F., Silenzi, S. 2007. Variazioni relative del livello del mare e vulnerabilità delle pianure costiere italiane. Quaderni della Societa Geologica Italiana 2, 1-29 (in Italian).

[3] Benac, Č., Juračić, M. 1998. Geomorphological indicators of sea level changes during upper Pleistocene (Würm) and Holocene in the Kvarner region (NE Adriatic Sea). Acta Geographica Croatica 33, 27-45.

[4] Benac, Č., Juračić, M., Bakran-Petricioli, T. 2004. Submerged tidal notches in the Rijeka Bay NE Adriatic Sea: Indicators of relative sea-level change and of recent tectonic movements. Marine Geology 212, 21-33.

[5] Benac, Č., Juračić, M., Matičec, D., Ružić, I., Pikelj, K. 2013. Fluviokarst and classical karst: Examples from the Dinarics (Krk Island, Northern Adriatic,
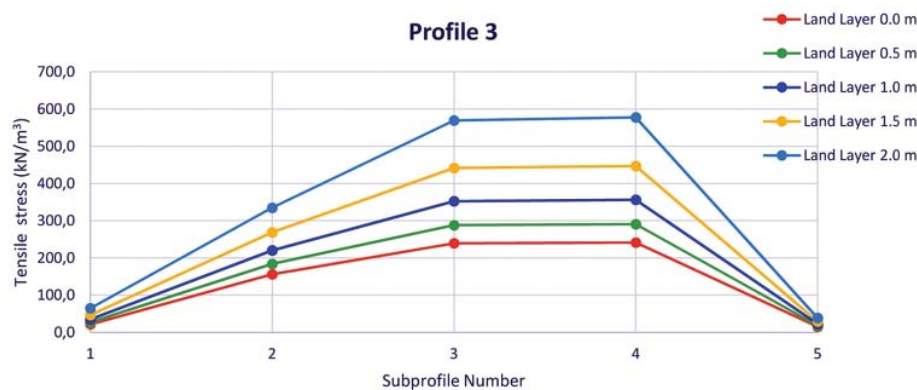

Figure 10. Different soil layer (on the top of the cliff, Fig. 3) height and cliff critical profile tensile stresses (profiles 3–1 to 3–5).

Croatia). Geomorphology 184, 64-73.

[6] Booij, N., Ris, R.C., Holthuijsen, L.H. 1999. A third-generation wave model for coastal regions, Part I: Model description and validation. Journal of Geophysical Research 104 (C4), 7649-7666.

[7] Castedo, R., Murphy, W., Lawrence, J., Parede, C. 2012. A new process-response coastal recession model of soft rock cliffs. Geomorphology 178, 128-143.

[8] Davies, P., Williams, A.T., Bomboe, P. 1991. Numerical modelling of Lower Lias rock failures in the coastal cliffs of South Wales. Coastal Sediments '91. - American Society of Civil Engineers, New York, pp. 1599-1612.

[9] Griggs, G.B., Trenhaile, A.S. 1997. Coastal cliffs and platforms. Coastal Evolution: Late Quaternary shoreline morphodynamics, Cambridge, pp. 425-450.

[10] Hoek, E., Brown, E.T. 1991. Practical Estimates of Rock Mass Strength. International Journal of Rock Mechanics and Mining Science 34, 8, 1165-1187.

[11] Hoek, E. 1996. Strength of Rock and Rock Masses. ISRM News Journal 2, 2, 4-16.

[12] Hungr, O., Evans, S.G., Bovis, M., Hutchinson, J.N. 2001. Review of the classification of landslides of the flow type. Environmental and Engineering Geoscience 7, 221-238.

[13] James, M.R., Robson, S. 2012. Straightforward reconstruction of 3D surfaces and topography with a camera: Accuracy and geoscience application. Journal of Geophysical Research - Earth Surface 117(F3), F03017. doi:10.1029/2011JF002289.

[14] James, M.R., Ilić, S., Ružić, I. 2013. Measuring 3D coastal change with a digital camera. Proc. of the Coastal Dynamics 2013. - 7th International Conference on Coastal Dynamics, Arcachon, pp. 893-904.

[15] Juračić, M., Benac, Č., Pikelj, K., Ilić, S. 2009. Comparison of the vulnerability of limestone (karst) and siliciclastic coasts (example from the Kvarner area, NE Adriatic, Croatia). Geomorphology 107, 1-2, 90-99.

[16] Kogure, T., Aoki, H., Maekade, A., Hirose, T., Matsukura, Y. 2006. Effect of the development of notches and tension cracks on instability of limestone coastal cliffs in the Ryukyus, Japan. Geomorphology 80, 3-4, 236-244.

[17] Kogure, T., Matsukura, Y. 2010. Critical notch depths for failure of coastal limestone cliffs: case study at Kuro-shima Island, Okinawa, Japan. Earth Surface Processes and Landforms 35, 9, 1044–1056.

[18] Kuhn, D., Prüfer, S. 2014. Coastal cliff monitoring and analysis of mass wasting processes with the application of terrestrial laser scanning: A case study of Rügen, Germany. Geomorphology 213, 153-165.

[19] Leder, N., Smirčić, A., Vilibić, I. 1998. Extreme values of surface wave heights in the Northern Adriatic. Geofizika 15, 1, 1–13.

[20] Marinos, P., Hoek, E. 2000. GSI: A geologically friendly tool for rock mass strength estimation. Proceedings of the GeoEng 2000, Melbourne, pp. 1422-1446.

[21] Matsukura, Y. 1988. Cliff instability in pumice flow deposits due to notch formation on the Asama mountain slope, Japan. Zeischrift für Geomorpologie 32, 129-141.

[22] Matsukura, Y. 2001. Rockfall at Toyohama Tunnel, Japan, in 1996: effect of notch growth on instability of a coastal cliff. Bulletin of Engineering Geology and the Environment 60, 285-289.

[23] Pikelj, K., Juračić, M. 2013. Eastern Adriatic Coast (EAC): Geomorphology and Coastal Vulnerability of a Karstic Coast. Journal of Coastal Research 29, 4, 944-957.

[24] Podobnikar, T. 2009. Methods for visual quality assessment of a digital terrain model. S.A.P.I.EN.S [Online], 2, 2, URL: http://sapiens.revues.org/738 [accessed on April 4th 2014]

[25] Ružić, I. 2003. Analysis of the Sea level interaction with the rivers high water levels in the North Adriatic, the Dubračina mouth example. BSc thesis, University of Rijeka, Faculty of Civil Engineering, Rijeka, (in Croatian).

[26] Ružić, I., Marović, I., Vivoda, M., Dugonjić Jonjčević, S., Kalajžić, D., Benac, Č., Ožanić, N. 2013. Application of Structure-from-Motion photogrammetry for erosion processes monitoring, Moscenicka Draga example. Proc. of the 4th Workshop of the Japanese-Croatian Project on "Risk Identification and Land-Use Planning for Disaster Mitigation of Landslides and Floods in Croatia, University of Split, Split, pp. 49-50.

[27] Ružić. I., Marović, I., Benac, Č., Ilić, S. (2014). Coastal cliff geometry derived from structure-from-motion photogrammetry at Stara Baška, Krk Island, Croatia. Geo-Marine Letters. doi 10.1007/s00367-014-0380-4.

[28] Snavely, N., Seitz, S.N., Szeliski, R. 2008. Modeling the world from internet photo collections. International Journal of Computer Vision 80, 189-210.

[29] Sunamura, T. (1992). Geomorphology of Rocky Coasts. Wiley, Chichester.

[30] Thorne, C.R., Tovey, N.K. 1981. Stability of composite river banks. Earth Surface Processes and Landforms 6, 469-484.

[31] Timoshenko, S.P., Gere, J.M. 1972. Mechanics of Materials. Van Nostrand Reinhold Co., New York.

[32] Trenhaile, A.S. 2002. Rock coasts, with particular emphasis on shore platforms. Geomorphology 48, 1-3, 7-22.

[33] Westoby, M.J., Brasington, J., Glasser, N.F., Hambrey, M.J., Reynolds, J.M. 2012. "Structure-from-Motion" photogrammetry: A low-cost, effective tool for geoscience applications. Geomorphology 179, 300-314.

[34] Williams, A.T., Davies, P., Bomboe, P. 1993. Geometrical simulation studies of coastal cliff failures in Liassic strata, South Wales, UK. Earth Surface Processes and Landforms 18, 703-720.